CHEMISTRY OF MATERIALS

Article

pubs.acs.org/cm

Effect of Copolymer Composition on Electronic Conductivity of Electrochemically Oxidized Poly(3-hexylthiophene)-*b*-poly(ethylene oxide) Block Copolymers

Mahesh P. Bhatt,[‡,§,∥] Jacob L. Thelen,[‡,§,∥] and Nitash P. Balsara*[,†,‡,§,∥]

[†]Environmental Energy Technologies Division, [‡]Materials Sciences Division, and [∥]Joint Center for Energy Storage Research (JCESR), Lawrence Berkeley National Laboratory, Berkeley, California 94720, United States

[§]Department of Chemical and Biomolecular Engineering, University of California, Berkeley, California 94720, United States

ABSTRACT: This is a study of the effect of copolymer composition on the electronic conductivity of poly(3-hexylthiophene)-*b*-poly(ethylene oxide) (P3HT-*b*-PEO) block copolymers. A wide variety of P3HT-*b*-PEO block copolymers with P3HT volume fraction ranging from 0.28 to 0.86 were synthesized. Lithium bis(trifluoromethanesulfonyl) imide (LiTFSI) salt was added to the P3HT-*b*-PEO copolymers to enable electrochemical oxidation. Three terminal electrochemical cells were used to oxidize the P3HT microphase; the two outer electrodes were used to oxidize P3HT, while a nickel mesh located within the P3HT-*b*-PEO enabled measurement of electronic conductivity by ac impedance. Symmetric block copolymers with P3HT volume fractions in the vicinity of 0.5 exhibited the highest electronic conductivity in the oxidized state. The symmetric copolymers also exhibited the highest crystallinity. The intrinsic conductivity of oxidized P3HT microphases increases exponentially with increasing crystallinity.

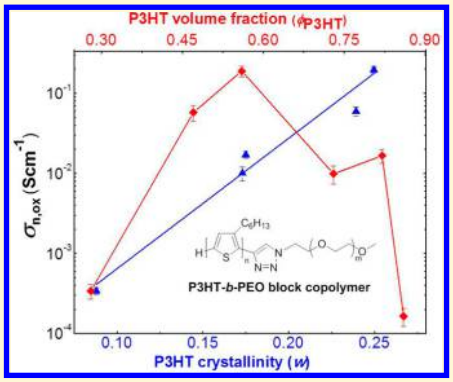

INTRODUCTION

Conjugated polymers that are electronically conductive have been studied extensively due to their potential applications such as organic solar cells,[1−8] flexible transistors,[9−13] and diodes.[14−18] These polymers are insulators in the pristine state, but they conduct electrons in the doped state.[16,19−21] Recent studies have explored the possibility of using these polymers to conduct electrons for enabling redox reactions in the electrodes of energy storage devices.[22−25] However, enabling redox reactions also requires transport of ions. Thus, there is interest in coupling electronically conducting polymers such as P3HT to an ionically conducting polymers such as poly(ethylene oxide) (PEO).[25] Like most block copolymer systems,[8,26−32] P3HT-*b*-PEO copolymers undergo microphase separation because of the incompatibility of the two blocks.[25,33−36] This results in the formation of P3HT-rich and PEO-rich nanoscale domains that can, in principle, provide pathways for simultaneous conduction of electrons and ions. The efficacy of P3HT-*b*-PEO copolymers as conducting binders in lithium battery cathodes has already been demonstrated.[25,35,36] In these systems, a salt such as lithium bis(trifluoromethanesulfonyl) imide salt (LiTFSI) is added to the P3HT-*b*-PEO copolymers to enable conduction of lithium ions.

The availability of well-defined ion conducting pathways enables electrochemical oxidation of P3HT domains, transforming them from insulators to conductors. Patel et al. developed a three-terminal cell to study the conductivity of the P3HT domains while monitoring the extent of electrochemical oxidation.[35] In this paper, we use these cells to study the effect of electrochemical oxidation on a wide variety of P3HT-*b*-PEO copolymers. The volume fraction of the P3HT block was varied from 0.28 to 0.86, and the molecular weight of the P3HT block was varied from 6 to 14 kg/mol. We show that the conductivity of oxidized P3HT is a sensitive function of the volume fraction of the P3HT block, ϕ_{P3HT}. Symmetric copolymers with $\phi_{P3HT} \approx 0.5$ exhibit the highest electronic conductivities in the oxidized state. In addition to electronic conductivity we also report on the morphology, thermal properties, and ionic conductivities of the copolymers. We found a strong correlation between electronic conductivity and crystallinity determined by differential scanning calorimetry.

Numerous papers have been written on the factors that control electronic transport in solvent processed P3HT thin films.[9,10,19,37−47] In these studies, carrier mobility in oxidized P3HT is measured, using either field-effect transistors or four point probes. Such measurements are necessarily restricted to thin films due to the limited diffusivity of dopants. In contrast, the presence of nanoscale channels for the introduction and removal of dopants in P3HT domains in our system allows us to probe bulk properties of samples as thick as 250 μm.[35,36] This is particularly relevant to electrical energy storage as the capacity of a battery to store and release energy is proportional to the thickness of the electrodes.

Received: June 2, 2015
Revised: July 1, 2015
Published: July 14, 2015

DOI: 10.1021/acs.chemmater.5b02085
Chem. Mater. 2015, 27, 5141−5148

EXPERIMENTAL SECTION

A series of P3HT-*b*-PEO block copolymers were synthesized by the combination of Grignard metathesis polymerization (GRIM) and a "click" reaction.[25] Azide-terminated PEO (PEO-azide) (number-averaged molecular weight, M_n = 2 kg/mol) was purchased from Polymer Source. An M_n = 10 kg/mol PEO-azide was obtained by end-group functionalization of monomethoxy-PEO that was purchased from Sigma-Aldrich.[48] Ethynyl terminated P3HT samples (M_n = 6, 10, 14 kg/mol) were synthesized by GRIM.[1] 1,3-Dipolar cylcoaddition click reactions between ethynyl terminated P3HT and PEO-azide were used to obtain the P3HT-*b*-PEO block copolymers listed in Table 1.

Table 1. Characteristics of the P3HT-*b*-PEO Block Copolymers

polymer	P3HT (M_n) (kg/mol)	PEO (M_n) (kg/mol)	ϕ_{P3HT}	σ_e (S cm^{-1}) (r_{ox} = 0.11)	*d*-spacing (nm)
P3HT-*b*-PEO (6-10)	6.1	10	0.28	9.71×10^{-5}	30
P3HT-*b*-PEO (10-10)	10.3	10	0.47	2.80×10^{-2}	22
P3HT-*b*-PEO (14-10)	14.2	10	0.56	1.03×10^{-1}	22
P3HT-*b*-PEO (6-2)	6.1	2	0.73	7.30×10^{-3}	29
P3HT-*b*-PEO (10-2)	10.3	2	0.82	1.14×10^{-2}	30
P3HT-*b*-PEO (14-2)[a]	14.2	2	0.86	1.42×10^{-4}	33

[a]Not completely oxidized due to limited LiTFSI in the sample.

Polymers are labeled P3HT-*b*-PEO(*x*-*y*), where *x* and *y* are the nominal molecular weights of the P3HT and PEO blocks in kg/mol. Polymers P3HT-*b*-PEO(6-2) and P3HT-*b*-PEO(10-2) were synthesized by the method described by Javier et al.[25] The other block copolymers were obtained by performing the click reactions at 70 °C using a 1:1 molar ratio of CuBr(I) and CuI(I) as a catalyst. The molecular weights (M_n) of ethynyl-P3HT and P3HT-*b*-PEO block copolymers, determined using ^{1}H NMR, are given in Table 1. A polystyene-*b*-poly(ethylene oxide) (PS-*b*-PEO) copolymer was purchased from polymer source. The M_n of the PS block was 386 kg/mol, and M_n of the PEO block was 300 kg/mol.

Mixtures of P3HT-*b*-PEO and LiTFSI were prepared in argon-filled gloveboxes (MBraun) following procedures described in ref 35. LiTFSI was purchased from Novolyte and dried under vacuum at 120 °C for 3 days. Neat P3HT-*b*-PEO samples were dried under vacuum at 90 °C overnight. LiTFSI/anhydrous THF mixtures were prepared at a concentration of 0.4 g/mL. The P3HT-*b*-PEO samples were dissolved in anhydrous benzene at a concentration of 5 mg/mL. The two solutions were mixed to obtain the desired salt concentration and stirred overnight. Next, the mixture was transferred to a custom built airtight desiccator in the glovebox. The desiccator was then connected to a Millrock LD85 lyophilizer located outside the glovebox for 3 days to dry the samples. The dry P3HT-*b*-PEO/LiTFSI mixtures were then taken into the antechamber of the glovebox, dried at 90 °C overnight, and taken into the glovebox. All the mixtures had the same salt concentration with r_0 = 0.085, where r_0 is the molar ratio of lithium to ethylene oxide units in the PEO block.

The poly(styrene)-*b*-poly(ethylene oxide) (PS-*b*-PEO) block copolymer was first dried in the glovebox antechamber under vacuum at 90 °C overnight. Then, in the glovebox, a mixture of PS-*b*-PEO and LiTFSI was dissolved in *N*-methyl-2-pyrrolidone (NMP 99.5% under Argon, EMD) and stirred at 90 °C for 6 h. The molar ratio of lithium ions (Li^+) to ethylene oxide (EO) moieties in our electrolyte, r_0, is 0.085. When the solution was clear and homogeneous, it was cast on a 201 annealed nickel (Ni) foil (All Foils, Inc.) using a doctor blade (Gardco) and a home-built casting device with a heated casting stage. The electrolyte film was obtained by drying at 65 °C for 12 h in the glovebox. The resulting membrane was peeled off from the Ni foil and dried in the glovebox antechamber under vacuum at 90 °C overnight. The PS-*b*-PEO electrolyte thickness was approximately 30 μm.

Ionic conductivities were measured in two terminal conductivity cells. Samples were prepared by hot pressing freeze-dried P3HT-*b*-PEO/LiTFSI into a 125 μm thick Garolite G-10 spacer with an inner-hole diameter of 0.476 cm. Nickel foil current collectors were pressed on both sides of the spacer at 90 °C. Nickel tabs were placed on both nickel foils. The samples were then sealed in aluminum laminated pouch material (Showa Denko) using a vacuum sealer (Packing Aids Corp).

Electronic conductivities were measured in three terminal cells as described by Patel et al.[35] A schematic of the cell is shown in Figure 1.

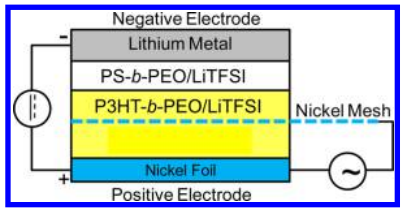

Figure 1. Schematic of a three terminal electrochemical cell.

The P3HT-*b*-PEO/LiTFSI mixture was pressed into two separate spacers described above. The polymer samples containing the 10 kg/mol PEO block were pressed at room temperature, while those containing 2 kg/mol PEO block were pressed at 90 °C because these copolymers have high P3HT content. The mass of the spacer was recorded before and after the addition of the polymer. The thickness, *L*, of each polymer filled spacer was measured (190−250 μm). An electroformed nickel mesh (Industrial Netting) was gently pressed between the two P3HT-*b*-PEO/LiTFSI films at either room temperature or 90 °C as described above. A nickel foil electrode was pressed on one side of the composite P3HT-*b*-PEO/LiTFSI films with the nickel mesh in the middle, while a piece of polymer electrolyte PS-*b*-PEO/LiTFSI membrane was pressed on the other side. A disk of lithium metal (150 μm) was gently pressed on the other side of the PS-*b*-PEO/LiTFSI polymer membrane. Nickel tabs were taped on the lithium, the nickel foil electrode, and the nickel mesh electrode. The samples were then sealed in pouch material using a vacuum sealer.

The three terminal cell shown schematically in Figure 1 enables simultaneous control over electrochemical doping of P3HT and its effect on electronic conductivity. The potentiostat between the negative and positive electrodes is used to drive dc current which results in electrochemical doping of P3HT. The potentiostat between the nickel mesh and the positive electrode is used to apply a small ac potential that is used to determine conductivity.

Galvanostatic oxidation experiments were performed using a Bio-Logic VMP3 potentiostat and the Bio-Logic EC-Lab data acquisition software. A constant current was applied between the negative lithium metal electrode and the nickel foil of the positive electrode to oxidize P3HT. The reactions that are assumed to occur in our cells are shown in Scheme 1.

It is well established that LiTFSI is fully dissociated in PEO matrices (electrolyte, Scheme 1).[49] We assume that Li^+ and $TFSI^-$ ions are transferred from the electrolyte into the negative and positive electrodes, respectively, when current is passed through the cells. The Li^+ ions participate in the plating reaction (negative electrode, Scheme 1). The $TFSI^-$ ions oxidize P3HT (positive electrode, Scheme 1). The oxidation level of P3HT is denoted as r_{ox}, the ratio of moles of electrons (e^-) transferred by the potentiostat to the moles of the 3-hexylthiophene moieties in the positive electrode. The moles of e^- transferred is given by

$$e^- = \frac{iAt}{F} \tag{1}$$

where *A* is the area of the sample (0.118 cm^2), *i* is current density (mA/cm^2) applied between the electrodes for a period of time *t*, and *F* is Faraday's constant. After reaching the desired r_{ox} value, electro-

DOI: 10.1021/acs.chemmater.5b02085
Chem. Mater. 2015, 27, 5141−5148

Scheme 1. Electrochemical Reactions Occurring in a Three Terminal Cell

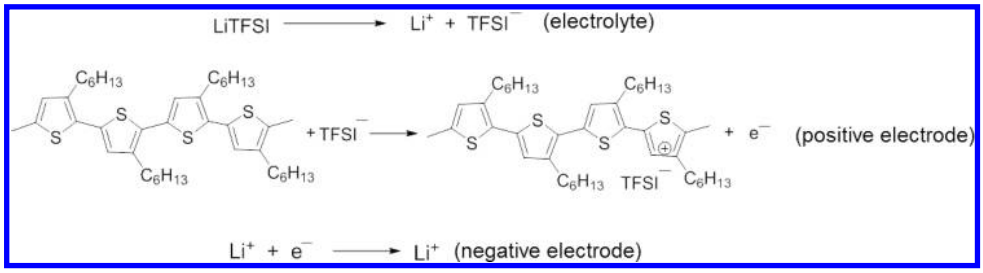

chemically oxidized cells were allowed to rest for 30 min prior to the impedance measurements. All samples were oxidized in steps from r_{ox} = 0 to r_{ox} = 0.13.

The impedance spectroscopy measurements were made using a Bio-Logics VMP3 potentiostat and Bio-Logics EC-Lab data acquisition software. The potentiostat was connected between the nickel mesh and nickel foil as shown in Figure 1. The magnitude of the applied ac voltage was 50 mV with frequencies ranging from 50 mHz to 1 MHz. Electronic resistance was calculated from the Nyquist plot ($-Z''$ *vs* Z' where Z'' and Z' are the imaginary and real impedances). The conductivity, σ, is given by

$$\sigma = \frac{L}{R} \tag{2}$$

where L is the polymer thickness, and R is the resistance ($\Omega \cdot cm^2$), obtained from intersections of the Nyquist plots on the Z' axis. All conductivity measurements were averaged over a minimum of three samples, and all reported error bars correspond to one standard deviation.

Small Angle X-ray Scattering (SAXS) samples were prepared by hot pressing freeze-dried P3HT-*b*-PEO block copolymer with LiTFSI into the spacer described above. SAXS measurements were taken at the Advanced Light Source (ALS) beamline 7.3.3 at Lawrence Berkeley National Lab. A silver behenate sample was used as a standard calibrant. The two-dimensional scattering patterns were collected on a 1 M Pilatus detector. The measured scattering data were averaged azimuthally to obtain intensity (I) versus magnitude of the scattering wave vector

$$q = \frac{4\pi}{\lambda}\sin\left(\frac{\theta}{2}\right) \tag{3}$$

where λ is the wavelength of the incident X-rays (0.124 nm), and θ is the scattering angle.

Differential scanning calorimetery (DSC) experiments were performed on a Thermal Advantage Q200 calorimeter at the Molecular Foundry, Lawrence Berkeley National Laboratory. Samples were sealed in aluminum hermetic pans in a glovebox. DSC scans consisted of two heating/cooling cycles and were conducted over the range −40 to 250 °C at a rate of 10 °C/min.

RESULTS AND DISCUSSION

The effect of electrochemical oxidation on P3HT-*b*-PEO(14-10)/LiTFSI and P3HT-*b*-PEO(6-10)/LiTFSI are shown in Figure 2, where Nyquist plots obtained at low and high oxidation levels are shown. At the low oxidation level (r_{ox} = 0.005), the Nyquist plots of both samples show three distinct features (Figures 2a and 2c). Our main objective is to estimate the electronic resistance, R_e, which is indicated in Figure 2. At the high oxidation level (r_{ox} = 0.11), the Nyquist plot shows only one feature with an electronic resistance that is orders of magnitude lower than at r_{ox} = 0.005. Figure 2 shows the range of data obtained from our samples: P3HT-*b*-PEO(14-10) shows the lowest electronic resistance, while P3HT-*b*-PEO(6-10) shows the highest resistance (r_{ox} = 0.11).

We expect the electronic conductivities of P3HT-*b*-PEO/LiTFSI at a given value r_{ox} to be proportional to the volume fraction of the P3HT microphase, ϕ_{P3HT}. We thus define a normalized electronic conductivity, $\sigma_{n,e}$, as

$$\sigma_{n,e} = \frac{\sigma_e}{\phi_{P3HT}} \tag{4}$$

where ϕ_{P3HT} is the volume fraction of the P3HT block in the neat P3HT-*b*-PEO block copolymers. In principle, ϕ_{P3HT} is the volume fraction of the P3HT-rich microphase in oxidized P3HT-*b*-PEO/LiTFSI mixtures, which is dependent on the concentration of $TFSI^-$ anions. Our analysis ignores the relatively small changes in volume fraction due to this effect.

In Figure 3a we plot the normalized electronic conductivities of P3HT-*b*-PEO(6-2) and P3HT-*b*-PEO(6-10) as a function of r_{ox}. (All oxidized samples contain LiTFSI. For simplicity, we do not explicitly mention this in the discussion below.) Both polymers show $\sigma_{n,e}$ values of about 10^{-6} S cm^{-1} at low oxidation levels. The normalized electronic conductivities of both polymers increase with increasing r_{ox} and reach plateaus when r_{ox} exceeds 0.09. The plateau value of $\sigma_{n,e}$ of P3HT-*b*-PEO(6-2) is a factor of 50 higher than that of P3HT-*b*-PEO(6-10) in spite of the fact that the molecular weight of P3HT blocks is identical in these two samples. It is evident that the volume fraction of the ionically conducting microphase affects the intrinsic properties of the electronically conducting microphase.

In Figure 3b we compare $\sigma_{n,e}$ vs r_{ox} data for polymers P3HT-*b*-PEO(10-2) and P3HT-*b*-PEO(10-10). These data are qualitatively similar to Figure 3a except for the fact that the high oxidation plateau is reached at r_{ox} = 0.11. In Figure 3c we compare $\sigma_{n,e}$ vs r_{ox} data for polymers P3HT-*b*-PEO(14-2) and P3HT-*b*-PEO(14-10). The $\sigma_{n,e}$ of oxidized P3HT-*b*-PEO(14-2) plateaus at a relatively low value of 2×10^{-4} S cm^{-1} at $r_{ox} \geq 0.07$. In contrast $\sigma_{n,e}$ of oxidized P3HT-*b*-PEO(14-10) plateaus at a relatively high value of 2×10^{-1} S cm^{-1} at $r_{ox} \geq 0.11$.

In most of our samples, the added salt, which we assume resides primarily in the PEO-rich microphase before oxidation, does not limit the extent to which P3HT microphase can be oxidized (see Scheme 1).[36] The only exception is P3HT-*b*-PEO(14-2). It can readily be shown that all of the lithium in the sample is consumed at r_{ox} = 0.07. The plateau seen in Figure 3c at r_{ox} = 0.07 for P3HT-*b*-PEO(14-2) is due to this effect. The plateaus seen in all other samples indicate that there is a threshold beyond which the intrinsic conductivity of P3HT microphases does not increase with increasing carrier concentration. It is interesting to note that this threshold oxidation level depends mainly on the molecular weight of P3HT block; it has a value of 0.07 when the P3HT block is 6 kg/mol and 0.11 when the P3HT block is 10 or 14 kg/mol.

DOI: 10.1021/acs.chemmater.5b02085
Chem. Mater. 2015, 27, 5141−5148

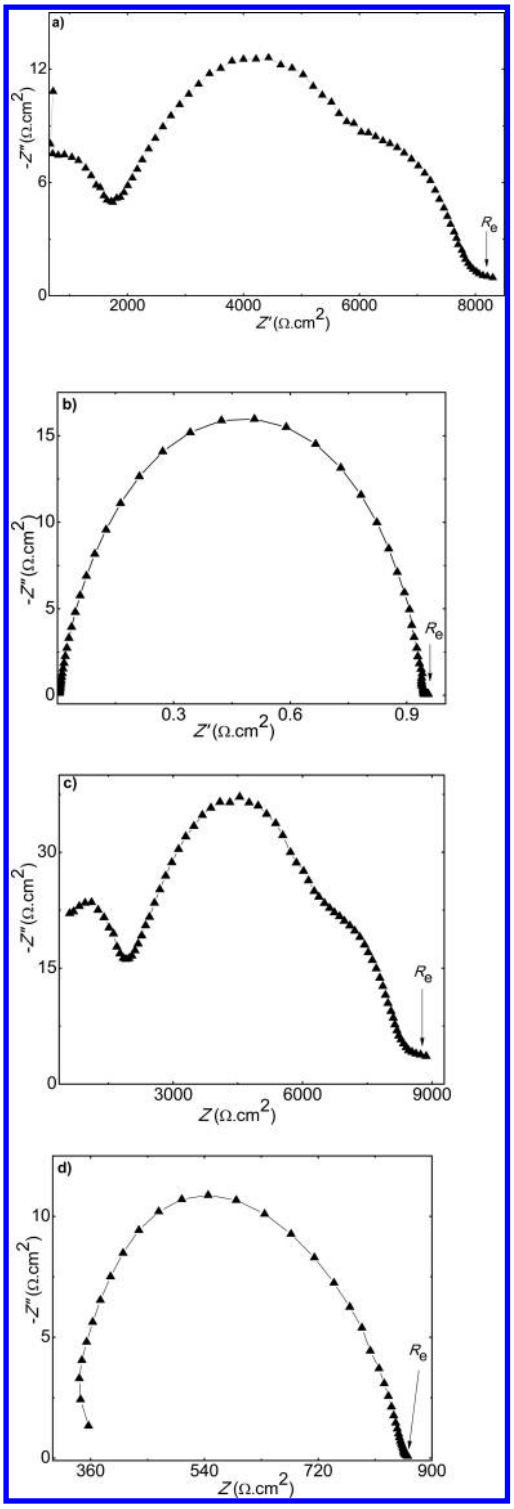

Figure 2. Characteristic Nyquist plot ($-Z''$ *vs* Z') of P3HT-*b*-PEO(14-10) at 90 °C **a)** r_{ox} = 0.005 and **b)** r_{ox} = 0.11. Characteristic Nyquist plot ($-Z''$ *vs* Z') of P3HT-*b*-PEO(6-10) at 90 °C **c)** r_{ox} = 0.005 and **d)** r_{ox} = 0.11.

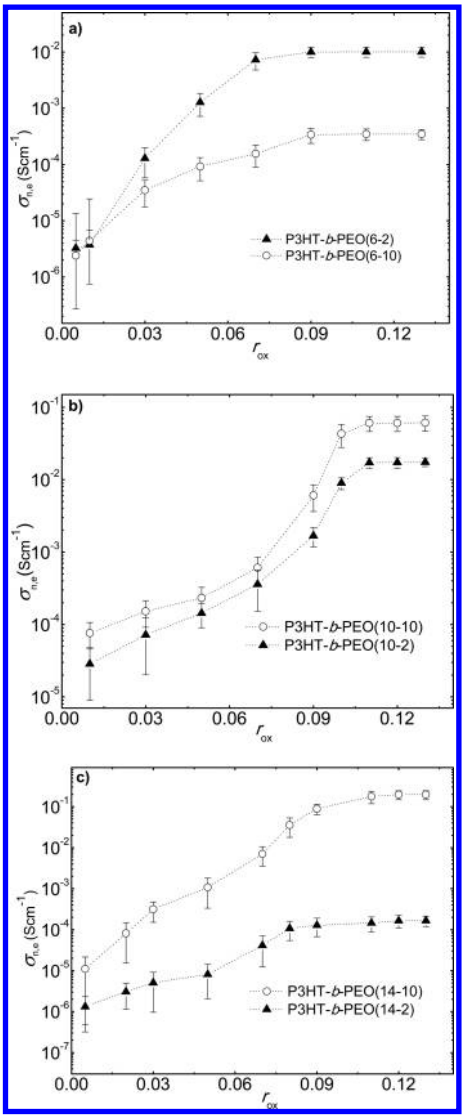

Figure 3. Electronic conductivities ($\sigma_{n,e}$) of the oxidized (a) P3HT-*b*-PEO(6-2), P3HT-*b*-PEO(6-10), (b) P3HT-*b*-PEO(10-2), P3HT-*b*-PEO (10-10), and (c) P3HT-*b*-PEO(14-2), P3HT-*b*-PEO (14-10) block copolymers at 90 °C for r_{ox} values ranging from 0.005 to 0.13.

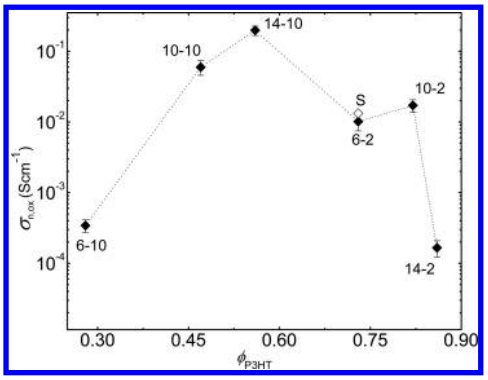

Figure 4. Electronic conductivities ($\sigma_{n,ox}$) of oxidized P3HT-*b*-PEO block copolymers as a function of volume fraction of P3HT (ϕ_{P3HT}) at r_{ox} = 0.11. S is taken from ref 35.

In Figure 4 we plot $\sigma_{n,ox}$, defined as the normalized electronic conductivity at r_{ox} = 0.11 vs ϕ_{P3HT}. Also included in this plot is data obtained from a P3HT-*b*-PEO(6-2) sample taken from Patel et al.[35] It is evident that $\sigma_{n,ox}$ is maximized in symmetric block copolymers with $\phi_{P3HT} \approx 0.5$. While electronic conductivity in the oxidized state is controlled mainly by block copolymer composition, overall molecular weight also plays a role. We see in Figure 4 that the electronic conductivity of P3HT-*b*-PEO(10-2) is higher than that of P3HT-*b*-PEO(6-2) in spite of the fact that P3HT-*b*-PEO(6-2) is closer to a

DOI: 10.1021/acs.chemmater.5b02085
Chem. Mater. 2015, 27, 5141−5148

symmetric composition. We explain this by proposing that the intrinsic conductivity of P3HT microphases increases with increasing P3HT molecular weight. We conclude that high molecular weight and symmetric P3HT-*b*-PEO copolymers exhibit the highest electronic conductivities.

Electron transport in block copolymers with an insulating block such as polyethylene and an electron transporting block such as P3HT has been extensively studied.[12,19,41,42,46,50−59] In most cases carrier mobilities were measured using field-effect transistors. In all these studies, conclusions about the effect of the block copolymer composition on electron transport have been made without normalizing the measured mobilities by ϕ_{P3HT}.[41,46,50−59]

P3HT-*b*-PEO copolymers contain nanoscale domains that transport ions and electrons in close proximity.[35] In fact, our ability to oxidize P3HT depends crucially on our ability to transport Li^+ and $TFSI^-$ in the PEO microphases; diffusion of $TFSI^-$ in P3HT is expected to be extremely slow. Data obtained from two terminal cells were used to estimate ionic conductivity in all of our P3HT-*b*-PEO/LiTFSI samples using the methodology established by Patel et al.,[35] and the results are shown in Figure 5a. The error bars for these measurements

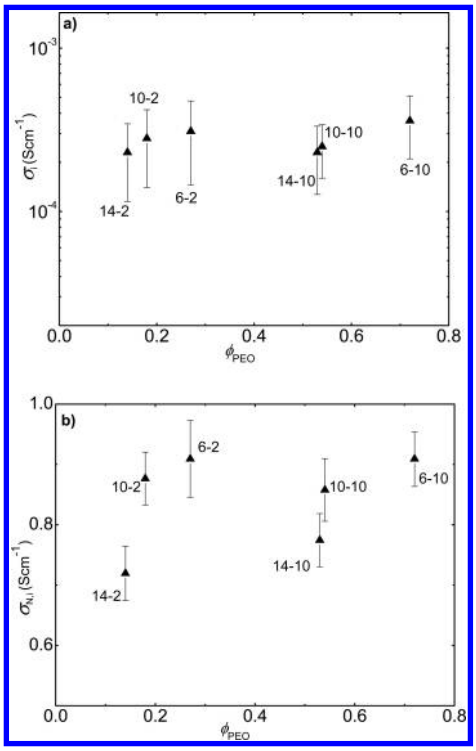

Figure 5. a) Ionic conductivities (σ_i) of P3HT-*b*-PEO/LiTFSI mixtures as a function of ϕ_{PEO}. b) Normalized ionic conductivities ($\sigma_{N,i}$) of P3HT-*b*-PEO/LiTFSI block copolymers as a function of ϕ_{PEO}.

are significant because the impedance spectra of unoxidized P3HT-*b*-PEO copolymers are dominated by the low electronic conductivity of the P3HT microphases.

The ionic conductivity of block copolymers with one ionically conducting microphase is proportional to the volume fraction of the conducting microphase. It is customary to define a normalized conductivity as follows

$$\sigma_{N,i} = \frac{\sigma_i}{f\phi_{PEO}\sigma_{PEO}} \tag{5}$$

where σ_i is the measured ionic conductivity of the block copolymer, ϕ_{PEO} is the volume fraction of the ionically conducting PEO microphase, σ_{PEO} is the ionic conductivity of PEO/LiTFSI mixtures at $r_0 = 0.085$, and f is a morphology factor that accounts for constraints imposed by the geometry of the conducting phase. We assume that $f = 2/3$, the value expected for a lamellar morphology. For P3HT-*b*-PEO samples with 2 kg/mol PEO blocks, $\sigma_{PEO} = 1.50 \times 10^{-3}$ S cm^{-1}, while for P3HT-*b*-PEO samples with 10 kg/mol PEO blocks, $\sigma_{PEO} = 2.20 \times 10^{-3}$ S cm^{-1}, as reported by Devaux and co-workers.[60] In Figure 5b we plot $\sigma_{N,i}$ vs ϕ_{PEO} ($\phi_{PEO} = 1 - \phi_{P3HT}$). The $\sigma_{N,i}$ values obtained in this study range between 0.7 and 1, consistent with the literature.[61−63]

Small angle x-ray scattering SAXS profiles of P3HT-*b*-PEO/LiTFSI mixtures are shown in Figure 6. The SAXS profiles of

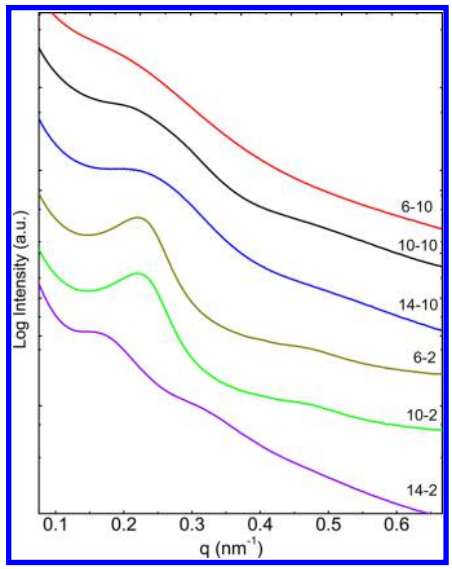

Figure 6. SAXS intensity versus scattering vector, q, of P3HT-*b*-PEO(6-10), P3HT-*b*-PEO(10-10), P3HT-*b*-PEO(14-10), P3HT-*b*-PEO(6-2), P3HT-*b*-PEO(10-2), and P3HT-*b*-PEO(14-2) with LiTFSI salt ($r_0 = 0.085$) obtained at 90 °C.

P3HT-*b*-PEO(6-2)/LiTFSI and P3HT-*b*-PEO(10-2)/LiTFSI show a primary peak at $q = q^* = 0.22$ nm^{-1} and 0.21 nm^{-1}, respectively. The profiles also show a higher order peak at $2q^*$, indicating the presence of a lamellar structure. The center-to-center distance between adjacent P3HT domains, d, can be calculated from

$$d = \frac{2\pi}{q^*} \tag{6}$$

The values of d for P3HT-*b*-PEO(6-2) and P3HT-*b*-PEO(10-2) are 29 and 30 nm, respectively. The SAXS profiles of all other polymers contain weak shoulders which we use to estimate d (Figure 6). The values of d thus obtained are given in Table 1. There appears to be no correlation between oxidized conductivities and morphology as determined by SAXS. For example, the SAXS profile of the sample that showed maximum conductivity [P3HT-*b*-PEO(14-10)] is similar to that obtained from the sample that showed the minimum conductivity [P3HT-*b*-PEO(14-2)]. The factor that affects oxidized conductivity is discussed below.

DOI: 10.1021/acs.chemmater.5b02085
Chem. Mater. 2015, 27, 5141−5148

Differential scanning calorimetry traces of all the P3HT-*b*-PEO/LiTFSI mixtures exhibited P3HT melting and crystallization peaks in the vicinity of 200 °C. The area under the crystallization peak was used to quantify the crystallinity of the P3HT microphases. Crystalline fraction, w, is given by the ratio of the measured enthalpy of crystallization per gram of P3HT to that of homopolymer P3HT (99 J/g).[64] The dependence of w on ϕ_{P3HT} is shown in Figure 7a. It is evident that w is

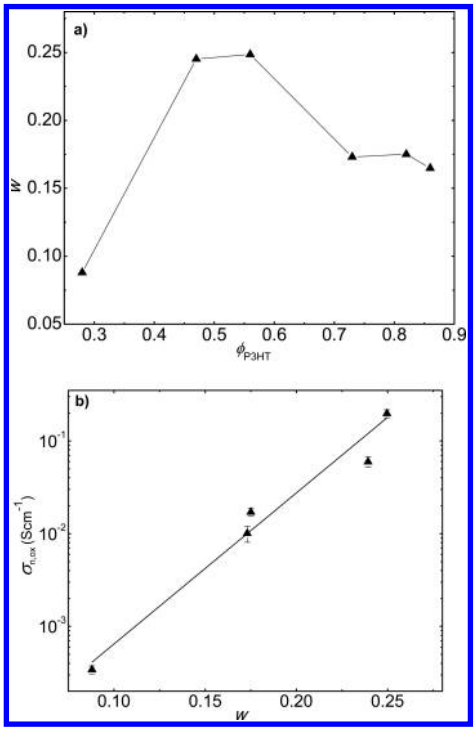

Figure 7. a) Crystallinity of P3HT (w), determined by DSC, in P3HT-*b*-PEO/LiTFSI mixtures (r_0 = 0.085) as a function of P3HT volume fraction (ϕ_{P3HT}). **b)** Electronic conductivities ($\sigma_{n,ox}$) of P3HT-*b*-PEO block copolymers as a function of P3HT crystallinity (w).

maximized in the case of symmetric block copolymers. This dependence is qualitatively similar to the dependence of $\sigma_{n,ox}$ on ϕ_{P3HT} (Figure 4). In Figure 7b we plot $\sigma_{n,ox}$ as a function of w on a semilog plot. We show data from all samples except P3HT-*b*-PEO(14-2) because oxidation of this sample was limited by salt availability. The data in Figure 7b suggests that $\log_{10}(\sigma_{n,ox})$ is a linear function of w. The line in Figure 7b is the least-squares linear fit through the data which indicates that $\log_{10}(\sigma_{n,ox}) = 0.16w - 4.81$ with an R^2 value of 0.98.

The fact that oxidized electronic conductivity P3HT-*b*-PEO samples depend only on crystallinity and not on morphology suggests that the geometry and connectivity of the conducting microphase is similar in all cases.

CONCLUSIONS

We have demonstrated that the electronic conductivity of electrochemically oxidized P3HT-*b*-PEO block copolymers is strongly influenced by the copolymer composition. Symmetric copolymers with $\phi_{P3HT} \approx 0.5$ exhibited high electronic conductivity in the fully oxidized state. Symmetric block copolymers also exhibited high crystallinity. We find a correlation between the intrinsic conductivity of oxidized P3HT microphases and crystallinity; intrinsic conductivity increases exponentially with increasing crystallinity.

AUTHOR INFORMATION

Corresponding Author

*Phone: 510.642.8937. Fax: 510.642.4778. E-mail: nbalsara@berkeley.edu.

Notes

The authors declare no competing financial interest.

ACKNOWLEDGMENTS

This work was primarily supported as part of the Joint Center for Energy Storage Research, an Energy Innovation Hub funded by the U.S. Department of Energy (DOE), Office of Science, Basic Energy Sciences (BES). X-ray scattering research at the Advanced Light Source was supported by DOE, Office of Science, BES. The electrochemical testing equipment was supported by the Assistant Secretary for Energy Efficiency and Renewable Energy, Office of Vehicle Technologies of the U.S. Department of Energy under Contract DE-AC02-05CH11231 under the Batteries for Advanced Transportation Technologies (BATT) Program. Work at the Molecular Foundry, Lawrence Berkeley National Laboratory was supported by DOE, Office of Science, BES under Contract DE-AC02-11231.

NOMENCLATURE

r_0	molar ratio of lithium ions (Li^+) to ethylene oxide (EO) moieties
r_{ox}	oxidation state
σ_e	electronic conductivity (S cm^{-1})
$\sigma_{n,e}$	normalized electronic conductivity at a given oxidation state (S cm^{-1})
$\sigma_{n,ox}$	normalized electronic conductivity at oxidized state ($r_{ox} \geq 0.11$) (S cm^{-1})
σ_i	ionic conductivity (S cm^{-1})
$\sigma_{N,i}$	normalized ionic conductivity (S cm^{-1})
σ_{PEO}	ionic conductivity of PEO (S cm^{-1})
ϕ_{P3HT}	volume fraction of P3HT
ϕ_{PEO}	volume fraction of PEO
f	morphology factor
w	crystallinity

REFERENCES

(1) Loewe, R. S.; Khersonsky, S. M.; McCullough, R. D. A simple method to prepare head-to-tail coupled, regioregular poly(3-alkylthiophenes) using Grignard metathesis. *Adv. Mater.* **1999**, *11*, 250−253.

(2) Loewe, R. S.; Ewbank, P. C.; Liu, J.; Zhai, L.; McCullough, R. D. Regioregular, Head-to-Tail Coupled Poly(3-alkylthiophenes) Made Easy by the GRIM Method: Investigation of the Reaction and the Origin of Regioselectivity. *Macromolecules* **2001**, *34*, 4324−4333.

(3) Greene, L. E.; Law, M.; Yuhas, B. D.; Yang, P. ZnO-TiO2 Core-Shell Nanorod/P3HT Solar Cells. *J. Phys. Chem. C* **2007**, *111*, 18451−18456.

(4) Chen, H.-Y.; Hou, J.; Zhang, S.; Liang, Y.; Yang, G.; Yang, Y.; Yu, L.; Wu, Y.; Li, G. Polymer solar cells with enhanced open-circuit voltage and efficiency. *Nat. Photonics* **2009**, *3*, 649−653.

(5) Boudouris, B. W.; Frisbie, C. D.; Hillmyer, M. A. Nanoporous Poly(3-alkylthiophene) Thin Films Generated from Block Copolymer Templates. *Macromolecules* **2008**, *41*, 67−75.

(6) Chang, Y.-T.; Hsu, S.-L.; Su, M.-H.; Wei, K.-H. Soluble phenanthrenyl-imidazole-presenting regioregular poly(3-octylthiophene) copolymers having tunable bandgaps for solar cell applications. *Adv. Funct. Mater.* **2007**, *17*, 3326−3331.

(7) Han, Y.-K.; Lee, Y.-J.; Huang, P.-C. Regioregularity Effects in Poly(3-hexylthiophene):PCBM-Based Solar Cells Incorporating Acid-

DOI: 10.1021/acs.chemmater.5b02085
Chem. Mater. 2015, 27, 5141−5148

Doped Polyaniline Nanotubes as an Interfacial Layer. *J. Electrochem. Soc.* **2009**, *156*, K37−K43.
(8) He, M.; Han, W.; Ge, J.; Yang, Y.; Qiu, F.; Lin, Z. All-conjugated poly(3-alkylthiophene) diblock copolymer-based bulk heterojunction solar cells with controlled molecular organization and nanoscale morphology. *Energy Environ. Sci.* **2011**, *4*, 2894−2902.
(9) Sirringhaus, H.; Brown, P. J.; Friend, R. H.; Nielsen, M. M.; Bechgaard, K.; Langeveld-Voss, B. M. W.; Spiering, A. J. H.; Janssen, R. A. J.; Meijer, E. W.; Herwig, P.; de Leeuw, D. M. Two-dimensional charge transport in self-organized, high-mobility conjugated polymers. *Nature* **1999**, *401*, 685−688.
(10) Sirringhaus, H.; Brown, P. J.; Friend, R. H.; Nielsen, M. M.; Bechgaard, K.; Langeveld-Voss, B. M. W.; Spiering, A. J. H.; Janssen, R. A. J.; Meijer, E. W. Microstructure-mobility correlation in self-organised, conjugated polymer field-effect transistors. *Synth. Met.* **2000**, *111*−*112*, 129−132.
(11) Dimitrakopoulos, C. D.; Malenfant, P. R. L. Organic Thin Film Transistors for Large Area Electronics. *Adv. Mater.* **2002**, *14*, 99−117.
(12) Fang, Y.-K.; Liu, C.-L.; Li, C.; Lin, C.-J.; Mezzenga, R.; Chen, W.-C. Synthesis, Morphology, and Properties of Poly(3-hexylthiophene)-block-Poly(vinylphenyl oxadiazole) Donor-Acceptor Rod-Coil Block Copolymers and Their Memory Device Applications. *Adv. Funct. Mater.* **2010**, *20*, 3012−3024.
(13) Sirringhaus, H.; Wilson, R. J.; Friend, R. H.; Inbasekaran, M.; Wu, W.; Woo, E. P.; Grell, M.; Bradley, D. D. C. Mobility enhancement in conjugated polymer field-effect transistors through chain alignment in a liquid-crystalline phase. *Appl. Phys. Lett.* **2000**, *77*, 406−408.
(14) Friend, R.; Burroughes, J.; Shimoda, T. Semiconducting polymers are moving out of the research lab and into the marketplace asindustry realizes the commercial potential of polymer-based LEDs, displays and photovoltaics. *Phys. World* **1999**, 35−40.
(15) Burroughes, J. H.; Bradley, D. D. C.; Brown, A. R.; Marks, R. N.; Mackay, R. N.; Friend, R. H.; Burns, P. L.; Holmes, A. B. Light-emitting diodes based on conjugated polymers. *Nature* **1990**, *347*, 539−541.
(16) Gross, M.; Muller, D. C.; Nothofer, H.-G.; Scherf, U.; Neher, D.; Brauchle, C.; Meerholz, K. Improving the performance of doped [pi]-conjugated polymers for use in organic light-emitting diodes. *Nature* **2000**, *405*, 661−665.
(17) Friend, R. H.; Gymer, R. W.; Holmes, A. B.; Burroughes, J. H.; Marks, R. N.; Taliani, C.; Bradley, D. D. C.; Santos, D. A. D.; Bredas, J. L.; Logdlund, M.; Salaneck, W. R. Electroluminescence in conjugated polymers. *Nature* **1999**, *397*, 121−128.
(18) Sirringhaus, H.; Tessler, N.; Friend, R. H. Integrated Optoelectronic Devices Based on Conjugated Polymers. *Science* **1998**, *280*, 1741−1744.
(19) Iovu, M. C.; Craley, C. R.; Jeffries-El, M.; Krankowski, A. B.; Zhang, R.; Kowalewski, T.; McCullough, R. D. Conducting Regioregular Polythiophene Block Copolymer Nanofibrils Synthesized by Reversible Addition Fragmentation Chain Transfer Polymerization (RAFT) and Nitroxide Mediated Polymerization (NMP). *Macromolecules* **2007**, *40*, 4733−4735.
(20) Jen, K. Y.; Miller, G. G.; Elsenbaumer, R. L. Highly conducting, soluble, and environmentally-stable poly(3-alkylthiophenes). *J. Chem. Soc., Chem. Commun.* **1986**, 1346−7.
(21) Romero, D. B.; Schaer, M.; Zuppiroli, L.; Cesar, B.; François, B. Effects of doping in polymer lightâ€ emitting diodes. *Appl. Phys. Lett.* **1995**, *67*, 1659−1661.
(22) Jeon, J.-W.; Kwon, S. R.; Lutkenhaus, J. L. Polyaniline nanofiber/electrochemically reduced graphene oxide layer-by-layer electrodes for electrochemical energy storage. *J. Mater. Chem. A* **2015**, *3*, 3757−3767.
(23) Kwon, S. R.; Jeon, J.-W.; Lutkenhaus, J. L. Sprayable, paintable layer-by-layer polyaniline nanofiber/graphene electrodes. *RSC Adv.* **2015**, *5*, 14994−15001.
(24) Shao, L.; Jeon, J.-W.; Lutkenhaus, J. L. Polyaniline nanofiber/vanadium pentoxide sprayed layer-by-layer electrodes for energy storage. *J. Mater. Chem. A* **2014**, *2*, 14421−14428.
(25) Javier, A. E.; Patel, S. N.; Hallinan, D. T.; Srinivasan, V.; Balsara, N. P. Simultaneous Electronic and Ionic Conduction in a Block Copolymer: Application in Lithium Battery Electrodes. *Angew. Chem., Int. Ed.* **2011**, *50*, 9848−9851.
(26) Tu, G.; Li, H.; Forster, M.; Heiderhoff, R.; Balk, L. J.; Sigel, R.; Scherf, U. Amphiphilic Conjugated Block Copolymers: Synthesis and Solvent-Selective Photoluminescence Quenching. *Small* **2007**, *3*, 1001−1006.
(27) Bellomo, E. G.; Wyrsta, M. D.; Pakstis, L.; Pochan, D. J.; Deming, T. J. Stimuli-responsive polypeptide vesicles by conformation-specific assembly. *Nat. Mater.* **2004**, *3*, 244−248.
(28) Cornelissen, J. J. L. M.; Donners, J. J. J. M.; de Gelder, R.; Graswinckel, W. S.; Metselaar, G. A.; Rowan, A. E.; Sommerdijk, N. A. J. M.; Nolte, R. J. M. Beta-Helical Polymers from Isocyanopeptides. *Science* **2001**, *293*, 676−680.
(29) Gu, Z.; Tan, Y.; Tsuchiya, K.; Shimomura, T.; Ogino, K. Synthesis and characterization of poly(3-hexylthiophene)-b-polystyrene for photovoltaic application. *Polymers* **2011**, *3*, 558−570.
(30) Han, D.; Tong, X.; Zhao, Y.; Zhao, Y. Block Copolymers Comprising Ï€-Conjugated and Liquid Crystalline Subunits: induction of Macroscopic Nanodomain Orientation. *Angew. Chem., Int. Ed.* **2010**, *49*, 9162−9165.
(31) He, M.; Qiu, F.; Lin, Z. Towards high performance organic-inorganic hybrid solar cells: bringing conjugated polymers and inorganic nanocrystals in close contact. *J. Phys. Chem. Lett.* **2013**, *4*, 1788−1796.
(32) He, M.; Qiu, F.; Lin, Z. Conjugated rod-coil and rod-rod block copolymers for photovoltaic applications. *J. Mater. Chem.* **2011**, *21*, 17039−17048.
(33) Shi, Y.; Li, F.; Chen, Y. Controlling morphology and improving the photovoltaic performances of P3HT/ZnO hybrid solar cells via P3HT-b-PEO as an interfacial compatibilizer. *New J. Chem.* **2013**, *37*, 236−244.
(34) Mohamed, M. G.; Cheng, C.-C.; Lin, Y.-C.; Huang, C.-W.; Lu, F.-H.; Chang, F.-C.; Kuo, S.-W. Synthesis and self-assembly of water-soluble polythiophene-graft-poly(ethylene oxide) copolymers. *RSC Adv.* **2014**, *4*, 21830−21839.
(35) Patel, S. N.; Javier, A. E.; Balsara, N. P. Electrochemically Oxidized Electronic and Ionic Conducting Nanostructured Block Copolymers for Lithium Battery Electrodes. *ACS Nano* **2013**, *7*, 6056−6068.
(36) Patel, S. N.; Javier, A. E.; Stone, G. M.; Mullin, S. A.; Balsara, N. P. Simultaneous Conduction of Electronic Charge and Lithium Ions in Block Copolymers. *ACS Nano* **2012**, *6*, 1589−1600.
(37) Jimison, L. H.; Toney, M. F.; McCulloch, I.; Heeney, M.; Salleo, A. Charge-Transport Anisotropy Due to Grain Boundaries in Directionally Crystallized Thin Films of Regioregular Poly(3-hexylthiophene). *Adv. Mater.* **2009**, *21*, 1568−1572.
(38) Joseph Kline, R.; McGehee, M. D.; Toney, M. F. Highly oriented crystals at the buried interface in polythiophene thin-film transistors. *Nat. Mater.* **2006**, *5*, 222−228.
(39) Salleo, A.; Kline, R. J.; DeLongchamp, D. M.; Chabinyc, M. L. Microstructural Characterization and Charge Transport in Thin Films of Conjugated Polymers. *Adv. Mater.* **2010**, *22*, 3812−3838.
(40) Verduzco, R.; Botiz, I.; Pickel, D. L.; Kilbey, S. M.; Hong, K.; Dimasi, E.; Darling, S. B. Polythiophene-block-polyfluorene and Polythiophene-block-poly(fluorene-co-benzothiadiazole): Insights into the Self-Assembly of All-Conjugated Block Copolymers. *Macromolecules* **2011**, *44*, 530−539.
(41) Wu, P.-T.; Ren, G.; Kim, F. S.; Li, C.; Mezzenga, R.; Jenekhe, S. A. Poly(3-hexylthiophene)-b-poly(3-cyclohexylthiophene): Synthesis, microphase separation, thin film transistors, and photovoltaic applications. *J. Polym. Sci., Part A: Polym. Chem.* **2010**, *48*, 614−626.
(42) Yu, X.; Xiao, K.; Chen, J.; Lavrik, N. V.; Hong, K.; Sumpter, B. G.; Geohegan, D. B. High-Performance Field-Effect Transistors Based on Polystyrene-b-Poly(3-hexylthiophene) Diblock Copolymers. *ACS Nano* **2011**, *5*, 3559−3567.

DOI: 10.1021/acs.chemmater.5b02085
Chem. Mater. 2015, 27, 5141−5148

(43) Goh, C.; Kline, R. J.; McGehee, M. D.; Kadnikova, E. N.; Fréchet, J. M. J. Molecular-weight-dependent mobilities in regioregular poly(3-hexyl-thiophene) diodes. *Appl. Phys. Lett.* **2005**, *86*, 122110.
(44) Kline, R. J.; DeLongchamp, D. M.; Fischer, D. A.; Lin, E. K.; Heeney, M.; McCulloch, I.; Toney, M. F. Significant dependence of morphology and charge carrier mobility on substrate surface chemistry in high performance polythiophene semiconductor films. *Appl. Phys. Lett.* **2007**, *90*, 062117−3.
(45) Kline, R. J.; McGehee, M. D.; Kadnikova, E. N.; Liu, J.; Fréchet, J. M. J. Controlling the Field-Effect Mobility of Regioregular Polythiophene by Changing the Molecular Weight. *Adv. Mater.* **2003**, *15*, 1519−1522.
(46) Iovu, M. C.; Jeffries-El, M.; Sheina, E. E.; Cooper, J. R.; McCullough, R. D. Regioregular poly(3-alkylthiophene) conducting block copolymers. *Polymer* **2005**, *46*, 8582−8586.
(47) Iovu, M. C.; Jeffries-El, M.; Zhang, R.; Kowalewski, T.; McCullough, R. D. Conducting block copolymer nanowires containing regioregular poly(3-hexylthiophene) and polystyrene. *J. Macromol. Sci., Part A: Pure Appl.Chem.* **2006**, *43*, 1991−2000.
(48) Scriven, E. F. V.; Turnbull, K. Azides: their preparation and synthetic uses. *Chem. Rev.* **1988**, *88*, 297−368.
(49) Lascaud, S.; Perrier, M.; Vallee, A.; Besner, S.; Prud'homme, J.; Armand, M. Phase Diagrams and Conductivity Behavior of Poly-(ethylene oxide)-Molten Salt Rubbery Electrolytes. *Macromolecules* **1994**, *27*, 7469−7477.
(50) Müller, C.; Goffri, S.; Breiby, D. W.; Andreasen, J. W.; Chanzy, H. D.; Janssen, R. A. J.; Nielsen, M. M.; Radano, C. P.; Sirringhaus, H.; Smith, P.; Stingelin-Stutzmann, N. Tough, Semiconducting Poly-ethylene-poly(3-hexylthiophene) Diblock Copolymers. *Adv. Funct. Mater.* **2007**, *17*, 2674−2679.
(51) Sommer, M.; Hüttner, S.; Steiner, U.; Thelakkat, M. Influence of molecular weight on the solar cell performance of double-crystalline donor-acceptor block copolymers. *Appl. Phys. Lett.* **2009**, *95*, 183308.
(52) Sivula, K.; Ball, Z. T.; Watanabe, N.; Fréchet, J. M. J. Amphiphilic Diblock Copolymer Compatibilizers and Their Effect on the Morphology and Performance of Polythiophene:Fullerene Solar Cells. *Adv. Mater.* **2006**, *18*, 206−210.
(53) Dattani, R.; Bannock, J. H.; Fei, Z.; MacKenzie, R. C. I.; Guilbert, A. A. Y.; Vezie, M. S.; Nelson, J.; de Mello, J. C.; Heeney, M.; Cabral, J. T.; Nedoma, A. J. A general mechanism for controlling thin film structures in all-conjugated block copolymer:fullerene blends. *J. Mater. Chem. A* **2014**, *2*, 14711−14719.
(54) Hiorns, R. C.; de Bettignies, B. R.; Leroy, J.; Bailly, S.; Firon, M.; Sentein, C.; Khoukh, A.; Preud'homme, H.; Dagron-Lartigau, C. High molecular weights, polydispersities, and annealing temperatures in the optimization of bulk-heterojunction photovoltaic cells based on poly(3-hexylthiophene) or poly(3-butylthiophene). *Adv. Funct. Mater.* **2006**, *16*, 2263−2273.
(55) Kruger, R. A.; Gordon, T. J.; Baumgartner, T.; Sutherland, T. C. End-group functionalization of poly(3-hexylthiophene) as an efficient route to photosensitize nanocrystalline TiO2 films for photovoltaic applications. *ACS Appl. Mater. Interfaces* **2011**, *3*, 2031−2041.
(56) Ge, J.; He, M.; Qiu, F.; Yang, Y. Synthesis, Cocrystallization, and Microphase Separation of All-Conjugated Diblock Copoly(3-alkylthiophene)s. *Macromolecules* **2010**, *43*, 6422−6428.
(57) Izuhara, D.; Swager, T. M. Poly(3-hexylthiophene)-block-poly(pyridinium phenylene)s: Block Polymers of p- and n-Type Semiconductors. *Macromolecules* **2011**, *44*, 2678−2684.
(58) Palaniappan, K.; Hundt, N.; Sista, P.; Nguyen, H.; Hao, J.; Bhatt, M. P.; Han, Y.-Y.; Schmiedel, E. A.; Sheina, E. E.; Biewer, M. C.; Stefan, M. C. Block copolymer containing poly(3-hexylthiophene) and poly(4-vinylpyridine): Synthesis and its interaction with CdSe quantum dots for hybrid organic applications. *J. Polym. Sci., Part A: Polym. Chem.* **2011**, *49*, 1802−1808.
(59) Kong, X.; Jenekhe, S. A. Block Copolymers Containing Conjugated Polymer and Polypeptide Sequences:Synthesis and Self-Assembly of Electroactive and Photoactive Nanostructures. *Macromolecules* **2004**, *37*, 8180−8183.
(60) Devaux, D.; Bouchet, R.; Glé, D.; Denoyel, R. Mechanism of ion transport in PEO/LiTFSI complexes: Effect of temperature, molecular weight and end groups. *Solid State Ionics* **2012**, *227*, 119−127.
(61) Teran, A. A.; Tang, M. H.; Mullin, S. A.; Balsara, N. P. Effect of molecular weight on conductivity of polymer electrolytes. *Solid State Ionics* **2011**, *203*, 18−21.
(62) Panday, A.; Mullin, S.; Gomez, E. D.; Wanakule, N.; Chen, V. L.; Hexemer, A.; Pople, J.; Balsara, N. P. Effect of Molecular Weight and Salt Concentration on Conductivity of Block Copolymer Electrolytes. *Macromolecules* **2009**, *42*, 4632−4637.
(63) Sax, J.; Ottino, J. M. Modeling of transport of small molecules in polymer blends: Application of effective medium theory. *Polym. Eng. Sci.* **1983**, *23*, 165−176.
(64) Malik, S.; Nandi, A. K. Crystallization mechanism of regioregular poly(3-alkyl thiophene)s. *J. Polym. Sci., Part B: Polym. Phys.* **2002**, *40*, 2073−2085.

DOI: 10.1021/acs.chemmater.5b02085
Chem. Mater. 2015, 27, 5141−5148